ASSESSMENT OF DISTRIBUTED NON-LINEAR FIBER MODELS

Anur Oumer[1,*], Adil Zekaria[1]

[1] *School of Civil and Environmental Engineering, Addis Ababa Institution of Technology, Addis Ababa, University , Addis Ababa, Ethiopia*

* Corresponding author. E-mail address: anur.oumer@aait.edu.et

DOI: https://doi.org/10.20372/zede.v41i.8622

ABSTRACT

The study evaluates existing numerical nonlinear modeling techniques used in seismic analysis. Experimentally tested RC bridge column specimens have been taken as a case study and modeled in OpenSees finite element software. The study shows that the distributed force-based (FB) fiber models provide a more accurate result in capturing the nonlinear behavior of the RC bridge column that exhibits strain-hardening behavior. In contrast, the distributed displacement-based (DB) fiber models overestimate the ultimate capacity of the RC bridge column for sections exhibiting strain-hardening behavior. The study shows that for nonlinear analysis using distributed displacement-based (DB) fiber models, members should be divided into several elements to capture the inelastic response accurately. For the section exhibiting strain-softening behavior, both the distributed force-based (FB) and displacement-based (DB) fiber models are affected by localization issues. To overcome the localization issues, three-level of regularizations have been compared: 1) Applying regularization only to concrete, 2) Applying regularization only to steel 3) Applying regularization to concrete and steel materials. The level of regularizations was observed to have a significant effect in capturing the softening behavior, such as concrete crushing/spalling or rupture of reinforcing steel bars.

Keywords: beam-column fiber models, Nonlinear-analysis, Strain-Hardening, Strain-Softening, Localization, Regularization

1. INTRODUCTION

The advancement in computing technologies and the application of performance-based engineering design requires accurate and efficient computational nonlinear beam-column models. Based on their efficiency and computational cost, the nonlinear models used in the seismic analysis are classified into the (a) global model, (b) discrete finite element model, and (c) microscopic finite element models [1]. The study investigates the second class of models based on discrete finite element models. In discrete finite element models, two inelastic beam-column models are primarily adopted: (a) lumped plasticity and (b) distributed plasticity. The early approach to model lumped plasticity is by introducing zero-length nonlinear springs at both ends of the member. In these models, a hysteresis backbone curve is required to define the properties of the hinge.

The distributed plasticity models allow inelastic deformation to occur anywhere along the length of the beam-column elements. The axial-moment interaction can be captured automatically by

integrating sectional force-deformation along the length of the element. The most common distributed plasticity models used in earthquake engineering are classical displacement-based and force-based beam-column elements [1, 2]. For the structures, in which failure is dominated by flexure, distributed plasticity has gained wide acceptance in earthquake engineering. However, softening or localization issues for such models are critical problems [3–5].

This paper investigates the localization issue with different material regularization techniques in distributed plasticity and suggests the best way to overcome mesh-dependent response. The effect of applying partial regularization only to concrete, only to steel or full regularization to both concrete and steel materials for structures exhibiting softening behaviour is investigated using force-based and displacement-based distributed plasticity models. Previous researches did not elaborate the significance of the application of partial localization and the consequence in capturing the post peak softening behaviour of reinforced concrete section.

2. REVIEW THE STATE OF ART

2.1 Fiber Based Distributed Plasticity Beam-Column Element

The fiber models are one of the recent techniques used to determine the inelastic responses of the beam-column elements by integrating nonlinear responses over the monitored cross-sections, as shown in Figure 1. The process can be achieved by discretizing the cross-section into a finite number of fibers. Each fiber contains constitutive laws of steel reinforcement, unconfined, and confined concrete materials, as shown in Figure 1 a. The assumption of the plane sections is taken into account by employing an Euler-Bernoulli beam theory, which ensures that the strains are distributed linearly across the cross-section [1]. The axial-moment interaction can be captured automatically by integrating sectional force-deformation along the length of the element.

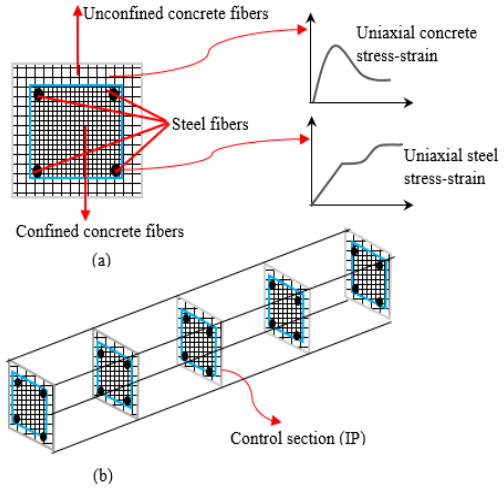

Figure 1 Distributed plasticity fiber-based beam-column element.

In the case of uniaxial bending the section stiffness matrix k_s can be evaluated numerically as follow:

$$k_s = \sum_{i=1}^{N_{IPs}} \begin{bmatrix} 1 & -y & z_i \\ -y_i & y_i^2 & y_i z_i \\ z_i & y_i z_i & z_i^2 \end{bmatrix} E_i w_i \qquad (1)$$

The section resisting forces s is calculated using the numerically integration as follow:

$$s = \begin{bmatrix} N \\ M_z \\ M_y \end{bmatrix} = \sum_{i=1}^{N_{IPs}} \begin{bmatrix} 1 \\ -y \\ z \end{bmatrix} \sigma_i w_i \qquad (2)$$

Where i is an integer counting from 1 to the number of integration points or (fibers) N_{IPs} And w_i is the weight of the integration scheme at i; E_i is the modulus of elasticity assigned to the integration point i.

2.1.1. Formulation of distributed displacement-based fiber models (DB)

The DB (displacement or stiffness-based) elements are the first distributed plasticity based on the classical stiffness method; thus, the models satisfy compatibility and equilibrium in an exact and approximate form, respectively. The models use a displacement interpolation function that assumes linear curvature and constant axial strain deformation to describe the nodal displacements. The element deformations are obtained directly from the shape function; hence iteration is required only at the structural level [1]. Figure2 shows that N, M_1, and M_2 are element forces denoted by q, and u, θ_1, and θ_2 are element deformations represented by v in the basic system.

Figure2 Basic forces of 2D beam-column element

$$u(x) = N(x)v \qquad (3)$$

Where u(x) is displacements at any point along the length of the beam-column element and $N(x)$ is a matrix containing the shape functions for the axial and transverse displacements.

$$\begin{bmatrix} u_1(x) \\ u_2(x) \end{bmatrix} = \begin{bmatrix} \frac{x}{L} & 0 & 0 \\ 0 & x - \frac{2x^2}{L} + \frac{x^3}{L^2} & -\frac{x^3}{L} + \frac{x^3}{L^2} \end{bmatrix} \begin{bmatrix} u \\ \theta_1 \\ \theta_2 \end{bmatrix} \qquad (4)$$

To ensure that the strains are distributed linearly across the cross-section, the first and second derivatives of the displacement shape functions must give constant axial strain and linear curvature, respectively, and are expressed as follows:

$$\begin{bmatrix} \varepsilon(x) \\ \kappa(x) \end{bmatrix} = \begin{bmatrix} \frac{\partial}{\partial x} & 0 \\ 0 & \frac{\partial^2}{\partial x^2} \end{bmatrix} \begin{bmatrix} u_1(x) \\ u_2(x) \end{bmatrix} \qquad (5)$$

The behavior of members near their ultimate resistance and the beginning of strain softening cannot be captured by the DB elements; hence multiple elements per member are needed to represent the inelastic response accurately [2,4,5]. Most recently, Pantò et al. [6] have introduced a new Smart Displacement Based (SDB) beam element to improve the accuracy of the standard DB element. "Smart" refers to an element's capacity to upgrade its displacement field following its current inelastic state [6]. According to the authors, the new model gives a result comparable to the FB models. Furthermore, Pantò et al. [7] extended the model to a Fibre Smart Displacement Based (FSDB) beam element to account for the axial force-bending moment interaction. A strong equilibrium of the axial force along the beam element, which is not often achieved by standard DB beam elements, is demonstrated to be possible with the Fibre Smart Displacement Based (FSDB) beam element [7]. Since those concepts are new and have yet to be incorporated in the

most known finite element softwares, this study focuses only on the standard DB elements.

2.1.2. Formulation of distributed force-based fiber models (FB)

In the FB (force or flexibility-based) approach, the force interpolation functions are used as a shape function. The force-based method is based on an exact equilibrium solution within the basic system of a beam-column element. Section forces are calculated using interpolation within the basic system from basic forces, as shown in equation (6):

$$s(x) = b(x)q \qquad (6)$$

Where b(x) is force interpolation functions that provide constant and linear distribution of axial force and bending moment, respectively for a member without distributed element loads:

$$b(x) = \begin{bmatrix} 1 & 0 & 0 \\ 0 & -\left(1-\frac{x}{L}\right) & \frac{x}{L} \end{bmatrix} \qquad (7)$$

The element state determination is more complex compared to the displacement-based fiber element. Element deformations in the basic system can be written as:

$$v = \int_0^L b^T(x)\ e(x)\, dx = \sum_{i=1}^{N_p} b_i^T e_i \omega_i \qquad (8)$$

The virtual force principle is used to derive the relationship between element deformations in the basic system v and sectional deformations e(x). Sectional deformation e(x) must be calculated from section forces s(x); however, in reality, this relation does not exist, but its inverse does [8, 9]. As a result, the section deformations are obtained by solving the nonlinear system of equations.

2.1.3. Localization issues in distributed fiber models

The term "localization" is well established in fracture mechanics, and various types of research are available regarding this topic. Experiment tests of compressive strength of different specimen sizes have shown that the post-peak stress-strain behavior of concrete is size-dependent. Jansen and Shah [10] conducted compressive tests for specimens with different slender lengths, and they found that the longer the specimen, the steeper the curves become. In computational mechanics, studies have shown that localization issues affect numerical models too; hence, this leads to the non-objective or mesh-dependent response, which results from the concentration of strain over a small finite element length or a single integration point. Before developing and applying force-based beam-column elements, localization issues have been primarily studied in displacement-based elements. Still, there are several regularization techniques in the literature for this model. Among the earliest studies, Bazant et al.[11] correctly recognized that the localization issue in the displacement-based element is sensitive to mesh size and the mean tangential bending stiffness. Zeris and Mahin [12] were the first to explain that softening in FB elements has different features from DB approaches. Deformations localize over a single

displacement-based element and single integration section in the DB and FB elements, respectively [13].

Even though several documented types of research on regularization techniques for DB are available, the works are more recent for FB beam-column elements. Coleman and Spacone [3] were the first who deeply investigated localization issues in FB beam-column model and applied the regularization techniques based on the constant fracture energy criterion to these models, which provides an objective response to the global force-displacement response. For sections undergoing softening, the FB element also fails to produce consistent and rational post-yielding global responses since the result is influenced by differences in the element mesh and the element's number of integration points. If too many integration points are employed, the element becomes unstable for softening sections [3, 5].

Coleman and Spacone [3]suggested a material regularization technique for FB models based on constant fracture energy criteria concepts to address mesh-dependent response. The authors modified the concrete model developed by Kent and Park [14] as shown in Figure 3.

The ultimate strain is adjusted at the quadrature integration points; then, the strain-softening process begins. The shaded area is proportional to the energy released after the pressure's softening. The idea is that the concrete material models assigned to distributed-plasticity fiber sections are modified to have constant dissipated material energy during crushing. The following expression is proposed to express ε_{20}:

$$\varepsilon_{20} = \frac{G_{fc}}{0.6 f_c' l_p} - \frac{0.8 f_c'}{E_c} + \varepsilon_c \qquad (9)$$

Where G_{fc} is the fracture energy of concrete in compression, f'_c is the compressive strength of the concrete, ε_c is peak compressive strain of the concrete, E_c is modulus of elasticity, ε_{20} is compressive strain corresponding to $20\%f'_c$ and L_p is length of the plastic hinge, which acts as the characteristic length to overcome mesh-dependent response.

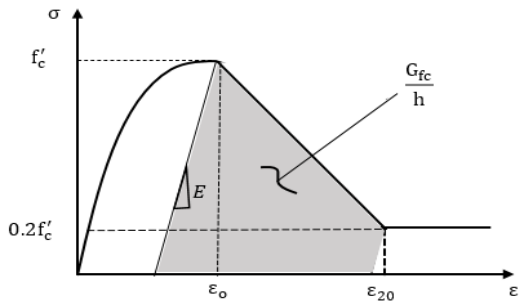

Figure 3 Kent–Park concrete stress–strain model with fracture energy in compression as shaded area

The regularization technique proposed by Coleman and Spacone [3]was applied only to distributed force-based beam-column model. Pugh [15] recently extended the work to include displacement-based fiber models. After conducting experimental tests on several planar wall specimens, Pugh [15] expressed the crushing energy value in the specified strength of unconfined and confined concrete.

Furthermore, he recommended using different crushing energy values for the force-based and displacement-based fiber beam-column models. He suggested the following values of unconfined crushing energy for the FB model:

$$G_{fc} = 2f_c'(\mathrm{N/mm}) \text{ (FB)} \qquad (10)$$

Applying the concrete crushing energies developed for the force-based beam-column element to the displacement-based element produces an over-prediction of drift capacity Pugh [15] . Therefore, for the DB element, the unconfined crushing energy is:

$$G_{fc} = 0.56f_c'(\mathrm{N/mm}) \text{ (DB)} \qquad (11)$$

The confined concrete crushing energy for both FB and DF models can be estimated as:

$$G_{fcc} = 1.7G_{fc} \qquad (12)$$

Then Equation 9 can be written for the confined concrete properties as:

$$\varepsilon_{20c} = \frac{G_{fcc}}{0.6f_{cc}'L_{IP}} - \frac{0.8f_{cc}'}{E_{cc}} + \varepsilon_{oc} \qquad (13)$$

Coleman and Spacone [3] recommended only applying material regularization techniques to the concrete material. However, this technique can be valuable only for sections subjected to high axial load, and failure is only due to concrete material crushing. If a member with widely spaced stirrups is subjected to high axial and cyclic lateral load, the section could face softening of concrete and localization of reinforcement bar. Reinforced concrete members at the critical section post-peak behavior of steel show strain hardening, whereas concrete exhibits strain softening. Even though steel shows hardening behavior, the section exhibits softening steel response and localizes at a critical section to confirm compatibility conditions[15,16]. Therefore, concrete and steel should be regularized because the section softening comes from the two fiber materials.

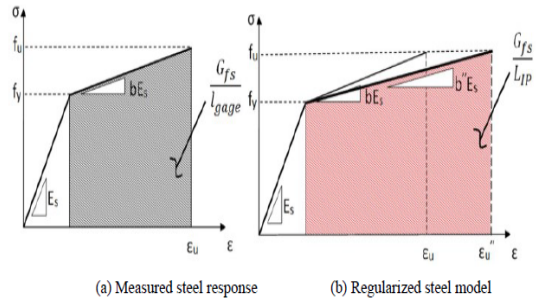

Figure 4 Stress-strain response histories for steel material [15]

The hardening energy, G_s for the simplified bi-linear steel stress-strain illustrated in Figurea can be defined as:

$$G_s = \frac{1}{2}(\varepsilon_{u,exp} - \varepsilon_y)(f_u - f_y)L_{gage} \qquad (14)$$

Where: $\boldsymbol{\varepsilon_{su}}$ is the rupture strain, $\boldsymbol{\varepsilon_y}$ is the yield strain, $\mathbf{f_u}$ is the ultimate tensile strength and $\mathbf{f_y}$ is the yield strength. The ultimate rupture strain assigned to the steel material model in the analysis should be updated based on the length associated with the critical section or element for regularizing the steel material. Using the Equation 14 and Figure 4b, the strain at ultimate strength, ε_u, used in defining the regularized model can be calculated as:

$$\varepsilon_u'' = \varepsilon_y + (\varepsilon_{u,exp} - \varepsilon_y)\frac{L_{gage}}{L_{IP}} \qquad (15)$$

As the mesh becomes more refined and small L_{IP}, the hardening modulus of the reinforcing steel decreases, requiring larger strains to reach a particular post-yield stress level Pugh [15]. It should be noted that these formulations neglect the curved transition between the initial and post-yielding hardening slopes specified by steel material developed by Menegotto and Pinto [17]; nonetheless, this is a minor simplification that was proven to have minimal impact on numerical findings [15]. The Gage length has been taken as 0.203 m, as suggested by ASTM A370 [15, 16]. After the ultimate strain is modified according to the gage length and length of the first integration section or element length, the post-yield hardening modulus must be modified based on the computed value for the maximum rupture strain of the regularized material [15, 16].

3. RESULTS AND DISCUSSION

3.1 Modelling Strategy

This section investigates the performance of the distributed force-based fiber models (FB) and displacement-based fiber models (DB) commonly used in earthquake engineering. The Open System for Earthquake Engineering Simulation, commonly known as OpenSees [18]finite element program, has been used to model a reinforced concrete bridge column downloaded from the PEER Structural Performance Database (2003). Material stress-strain relationships that describe the concrete and steel fibers should be adequately defined to capture the inelastic response of structures subjected to axial and lateral loading. To accurately simulate the bridge-reinforced concrete column specimens, the confined and unconfined concrete, denoted as Concrete02 in OpenSees, has been defined. The concrete Kent-Park model [14] shown in Figure 4was adopted to describe the stress-strain relation of concrete fibers. The monotonic compression envelope shown in Figure 5(a) has an initial parabolic envelope, a linear softening envelope, and an ultimate stress plateau. The confinement effect factor, K, can be determined using the formula proposed by Mander et al. [19]. For unconfined concrete fibers, the strain associated with 80% strength loss, f20u, was assumed to be 0.008. The ultimate strain capacity of the confined concrete can be calculated using Priestley et al. [20] expression as follows:

$$\varepsilon_{ccu} = 0.004 + 1.4\frac{\rho_s f_{yh}\varepsilon_{fs}}{f_{cc}} \qquad (16)$$

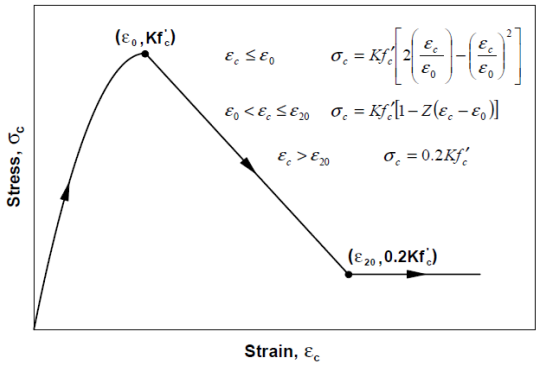

(a)

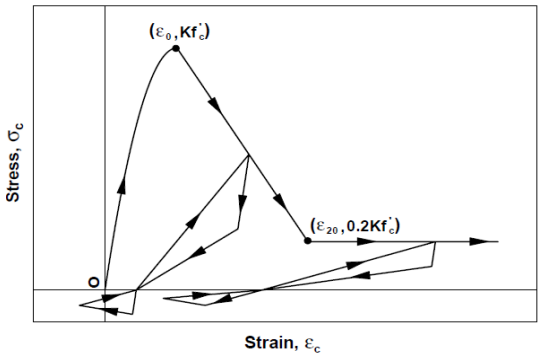

(b)

Figure 4 Yassin/Modified Park-Kent (a) monotonic (b) Cyclic envelope [15].

As illustrated in Figure 5(b), Yassin assigned bilinear unloading and linear reloading branches to implement cyclic behavior on the monotonic compression envelope [15]. These hysteretic rules assume that tensile response happens immediately after complete compression unloading and consider stiffness degradation throughout both unloading and reloading. It is assumed that cracks will close suddenly; this can be seen by the quick shift in stiffness that occurs when compression is reloaded, as shown in Figure 5(b). Both the post-cracking softness and tensile strength can be controlled [15].

Table 1 Properties of specimen A2 tested by Kunnath et al. [22].

Properties	Values
Concrete strength	29 (MPa)
Yield stress of stirrup	434 (MPa)
Yield stress of main bar	448 (MPa)
Diameter of the cross-section	305 (mm)
Height of the column	1372 (mm)
Test configuration	Cantilever
Axial load	200 (kN)
Diameter of the main bar	9.5 (mm)
Number of bars	21
Reinforcement ratio of the main bar	0.0204
Diameter of stirrup	4 (mm)
Hoop spacing, Sv	19 (mm)
Cover to center of hoop bar	14.5 (mm)
Reinforcement ratio of stirrup	0.94
Span-to-depth ratio	0.94
Axial load ratio	0.094

A steel material, Steel-02, with a bilinear steel envelope, has been used to define the reinforcement bar. Cyclic reinforcing steel behavior is commonly modeled using the Menegotto-Pinto-Filippou [21], which includes isotropic strain hardening, as shown in Figure 5.

This model represents steel behavior as a series of curved transitions between asymptotes defined by linear elastic and strain hardening properties. The curved transition allows for the representation of the Bauschinger effect. Model input parameters allow for control of cyclic stiffness deterioration.

3.2 Evaluation of DB and FB models under cyclic loading (Hardening)

Several researchers have identified that localization is not an issue for members exhibiting hardening behavior. The models are evaluated under members exhibiting strain-hardening behavior to verify these conclusions. Specimen A2 tested by Kunnath et al. [22] has been taken as a case study for a strain-hardening behavior. The axial load, cyclic lateral load, and section discretization of specimen A2 are indicated in Figure 6. The properties of specimen A2 have been summarized in Table 1. Table 2 shows the material properties used for modeling the specimen in OpeenSees finite element software.

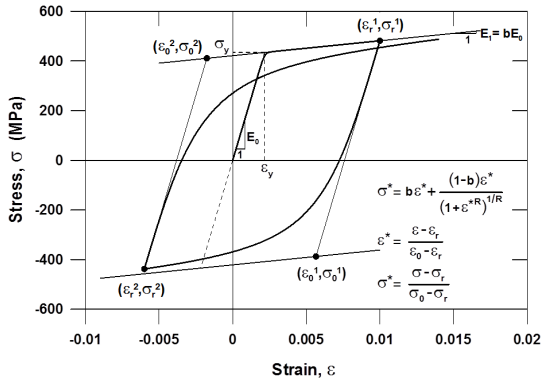

Figure 5 Menegotto-Pinto-Filippou model [21].

Strain-hardening behavior was considered because the column is subjected to a relatively low axial load of 200 kN

(0.09fc′Ac), as shown in Figure 6. Furthermore, the hysteresis response obtained from the experiment has not shown any softening or degradation in strength. The materials have been discretized into many concrete and steel fibers to integrate the uniaxial material along the section, as seen in Figure 6. To simulate the load applied during the experiment in OpenSees, first, a downward constant axial force of 200 kN is applied vertically through the force control loading. Once the gravity analysis has been carried out, the cyclic lateral load is applied through the displacement control.

Table 2 Material properties in OpenSeesof specimen A2 tested by Kunnath et al. [22]

Unconfined concrete(Concrete02)	
Maximum concrete strength (f_c')	29 Mpa
Peak strain (ε_{co})	$2\cdot\frac{f_{cc}}{E_{cc}}$
Crushing stress (f'_{c20})	$0.2\cdot f'_c$
Crushing strain (ε_{cu})	0.008
Confined concrete(Concrete02)	
Confinement factor (k)	1.62
compressive strength (f_{cc})	$k\cdot f'_c$
Peak strain (ε_{cco})	$2\cdot\frac{f_{cc}}{E_{cc}}$
Crushing stress (f_{cc20})	$0.2\cdot f_{cc}$
Crushing strain (ε_{ccu})	Equation 16
Reinforcement bar (Steel02)	
Yield strength(fy)	448 (mpa)
Modulus of elasticity (Es)	200000 (mpa)
Strain hardening	1%

For the section exhibiting strain-hardening behavior, cyclic analysis was carried out using the DB and the FB beam-column fiber models. Because Neuenhofer and Filippou [2] suggest that more integration points do not improve accuracy in the DB model, in this research, the member was divided into several elements with two Gauss-Legendre integration points. However, increasing the number of integration points for the force-based element has a significant impact on the numerical result; as a result, a single element of the force-based model with several integration points is used.

As shown in Figure 7, when mesh refinement increases, the cyclic moment-curvature does not converge into the same solution because the DB element formulation assumes linear curvature, which is valid only for elastic. As seen in Figure 8, convergence is achieved fast in the global response; however, the ultimate curvature still varies significantly in the local response (see Figure 7). As shown in Figure 8, the DB with one element highly overestimates the actual response compared to DB with 4 and 10 elements per member. The ultimate base shear of the experimental result is 73.97 kN. With a 56.82% error, the maximum base shear utilizing 1 DB element per member is 116 kN. However, the ultimate base shear is 75.74 kN (with a 2.33% error) when the member was refined to 4 and 10 DB elements per member.

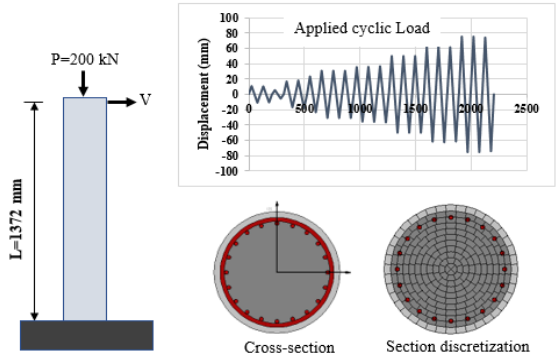

Figure 6 Simulation of axial load, cyclic lateral load and section discretization of the specimen A2 tested by Kunnath et al. [22].

Analysis using the FB fiber models shows that the cyclic moment-curvature converges into a unique solution for strain-hardening behavior with increased integration points, as shown in Figure 9. The FB models accurately capture the hysteresis force-deformation shape using only one element per member with few integration points, as shown in Figure 10. The FB captured the hysteresis curve of force-deformation response better than the displacement-based model. The ultimate base shear obtained using the FB element is 74.08 kN (with a 0.14% error), which is almost the same as the experimental value. The reason is that the FB model satisfies equilibrium in an exact sense, whereas the DB is average.

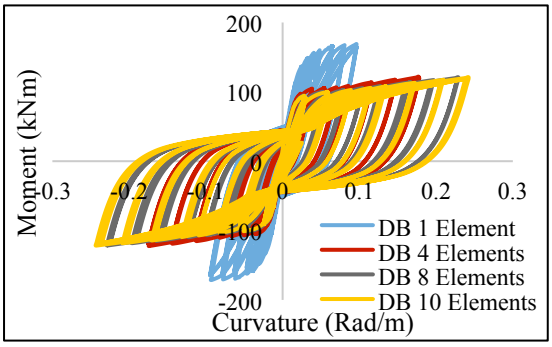

Figure 7 Hardening cyclic moment-curvature using DB (Specimen A2)

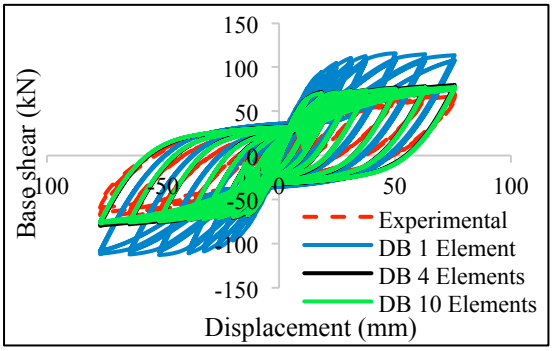

Figure 8 Hardening hysteresis response using DB (Specimen A2).

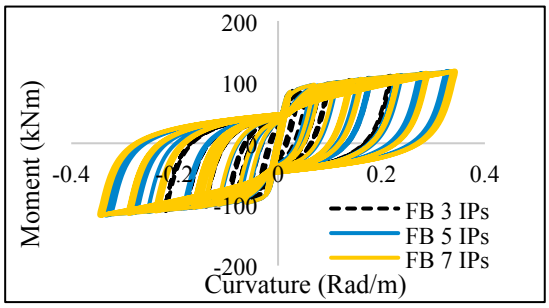

Figure 9 Hardening cyclic moment-curvature using FB (Specimen A2).

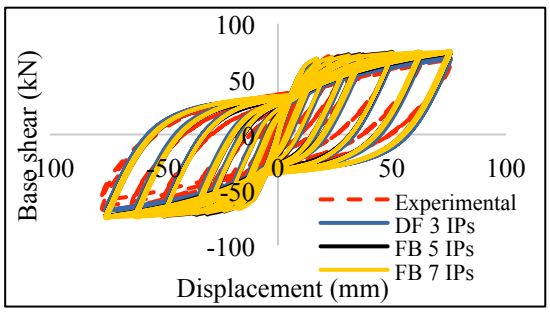

Figure 10 Hardening hysteresis response using FB (Specimen A2)

3.3 Evaluation of DB and DF models under monotonic loading (Softening)

Reinforced concrete columns that exhibit strain-softening behavior, specimen No. 3 in the tests by Wong et al. [23], and specimen FL3 tested by Kowalsky et al. [24], have been taken as the case study to show the effect of softening behavior on the performance of the distributed-based fiber models. Specimen No. 3 and specimen FL3 are subjected to a high axial load of 1813 kN and 1780 kN, respectively. For specimen No 3, the experimental test showed significant concrete spalling and longitudinal bar buckling at a drift of 1.21% (9.7 mm) and 3.23% (25.9 mm), respectively. For the specimen FL3, the experimental test showed significant concrete spalling and longitudinal bar buckling at a drift of 2.79 % (102 mm) and 9.3 % (340 mm), respectively.

For the push-over analysis, the loading method is carried out initially by applying a constant downward axial load through the force control loading. Then an increasing lateral monotonic load is applied through the displacement control. The Axial load, monotonic lateral load, and section discretization of specimen No. 3 are indicated in Figure 11. The actual properties of specimens No. 3 and FL3 have been summarized in Table 3.

Table 3 Actual Properties of specimen No. 3 [23] and specimen FL3[24].

Properties	Specimen No. 3	Specimen FL3
Concrete strength	37 (MPa)	38.6 (MPa)
Yield stress of stirrup	300 (MPa)	445 (MPa)
Yield stress of main bar	475 (MPa)	477 (MPa)
Diameter of the cross-section	400 (mm)	457 (mm)
Height of the column	800 (mm)	3,656 (mm)
Test configuration	Cantilever	Cantilever
Axial load	1813 (kN)	1,780 (kN)
Diameter of the main bar	16 (mm)	15.9 (mm)
Number of bars	20	30
Reinforcement ratio of the main bar	0.032	0.0362
Diameter of stirrup	10 (mm)	9.5 (mm)
Hoop spacing, Sv	60 (mm)	76 (mm)
Cover to center of hoop bar	20 (mm)	30.2 (mm)
Reinforcement ratio of stirrup	1.42	0.92
Span-to-depth ratio	2	8
Axial load ratio	0.39	0.281

A reinforced concrete column that exhibits strain-softening behavior was analyzed using FB and DB numerical models.

Figure **12**-Figure 15 show the monotonic response of the member analyzed using the FB and DB models for both specimens.

For the two specimens, the FB and DB numerical models showed two types of localization: first, linearly softening, which is the softening of concrete material that comes as the result of the crushing and spelling of concrete; second, a sudden drop in strength, which comes from the localization of the steel material (see Figure 13-Figure 16).

The analysis results have shown that mesh-dependent results underestimate the ultimate strength and drift capacity of the columns.

The softening rate in the DB model (see Figure 15 and Figure 16) is slow compared with the FB (see Figure 13 and Figure 14). On the other hand, the FB model's results began to soften with just one element (with 5 Ips), whereas the DB model experienced softening problems when the member was divided into eight or more elements (with 2 Ips).

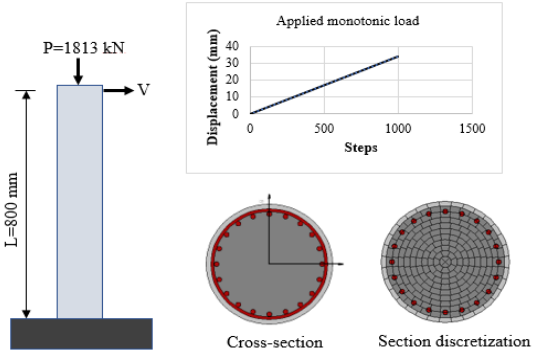

Figure 11 Axial load, monotonic lateral load and section discretization of specimenNo. 3.

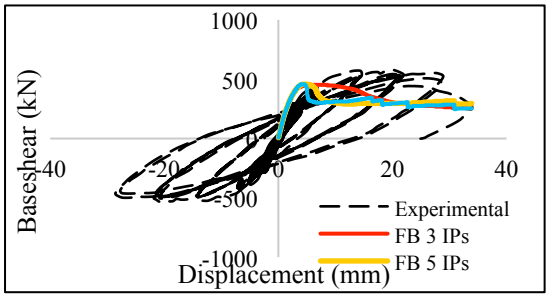

Figure 12 Monotonic response of specimen No. 3 using FB without applying material regularization.

Table 4 Material properties in OpenSees of specimen No. 3 [23] and specimen FL3 [24].

	Specimen No. 3	Specimen FL3
Unconfined concrete (Concrete02)		
Maximum concrete strength (f_c')	37 MPa	38.6 MPa
Peak strain (ε_{co})	$2\cdot\frac{f_{cc}}{E_{cc}}$	$2\cdot\frac{f_{cc}}{E_{cc}}$
Crushing stress (f_{c20}')	$0.2\cdot f_c'$	$0.2\cdot f_c'$
Crushing strain (ε_{cu})	0.008	0.008
Confined concrete (Concrete02)		
Confinement factor (k)	1.348	1.32
compressive strength (f_{cc})	$k\cdot f_c'$	$k\cdot f_c'$
Peak strain (ε_{cco})	$2\cdot\frac{f_{cc}}{E_{cc}}$	$2\cdot\frac{f_{cc}}{E_{cc}}$
Crushing stress (f_{cc20})	$0.2\cdot f_{cc}$	$0.2\cdot f_{cc}$
Crushing strain (ε_{ccu})	Equation 16	Equation 16
Reinforcement bar (Steel02)		
Yield strength(fy)	475 (MPa)	477 (MPa)
Modulus of elasticity (Es)	200000 (MPa)	200000 (MPa)
Strain hardening	1%	1%

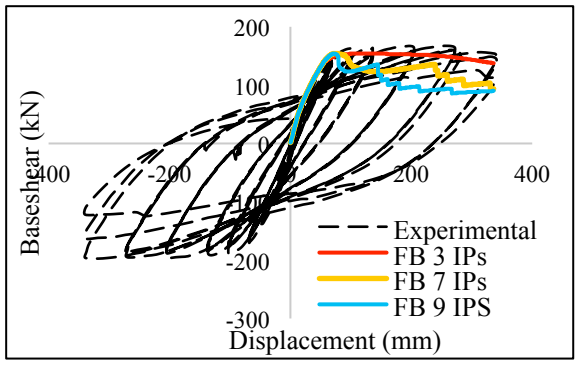

Figure 13 Monotonic response of specimenFL3 using FB without applying material regularization.

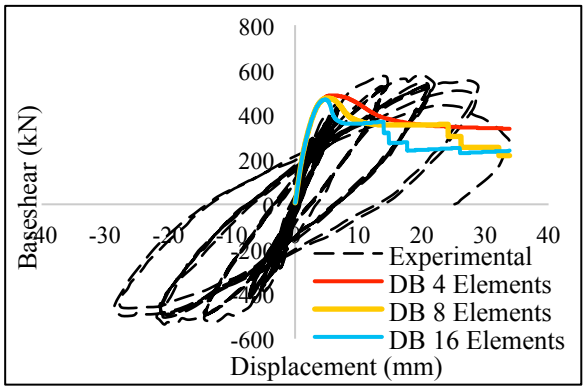

Figure 14 Monotonic response of specimen No. 3 using DB without applying material regularization.

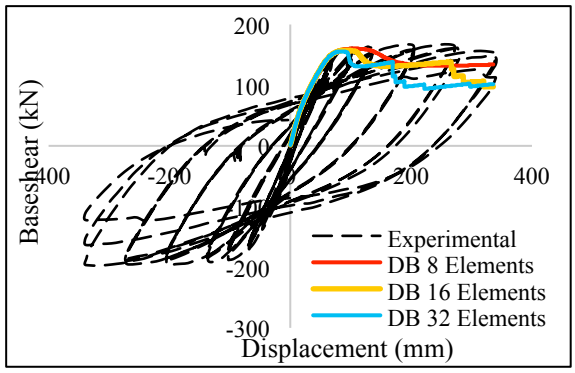

Figure 15 Monotonic response of specimen FL3 using DB without applying material regularization.

3.4 Investigation of partial and full material regularization in FB Model

Despite the fact that certain studies have suggested regularization be used for both steel and concrete materials, there hasn't been much discussion on the effect of the partial regularization techniques This

section briefly discusses partial and complete material regularization techniques for fiber beam-column elements. Coleman and Spacone [3] recommended material regularization only for the concrete section that fails due to concrete crushing. Later on, Pugh suggested including regularization for steel material [15]. The ultimate strain was modified using Equation 13 to regularize concrete material. Adjusted fracture strain for steel material calculated according to Equation 15. The gauge length was assumed to be 203 mm, as recommended by ASTM A370m, and the maximum strain was taken as 0.09. In OpenSees, MinMax criteria have been considered for the steel, which enforces the stiffness and strength of the steel fibers to become zero when the compressive strain is reached. The estimated properties of the regularized material for FB and DB are summarized in Table 5 and Table 6. This paper does not present softening issues and regularization techniques at the local level.

Table 5 Regularized strains of the unconfined and confined concrete, steel ultimate rupture strain and strain hardening of specimen No. 3for FB and DB models.

Force-based model (FB)					
No of Ips	LIP	ε_{c20}	ε_{cc20}	ε"	bs
3	133.3	0.027	0.034	0.136	0.006
7	40.0	0.085	0.109	0.447	0.002
9	19.0	0.177	0.227	0.936	0.001
Displacement-based model (DB)					
No of Elements	LIP	ε_{c20}	ε_{cc20}	ε"	bs
4	100	0.006	0.009	0.180	0.004
8	50	0.016	0.020	0.358	0.002
16	25	0.034	0.044	0.714	0.001

Table 6 Regularized strains of the unconfined and confined concrete, steel ultimate rupture strain and strain hardening of FL3 for FB and DB model.

Force-based model (FB)					
No of Ips	LIP	ε_{c20}	ε_{cc20}	ε"	bs
3	609.3	0.0071	0.0089	0.0316	0.0517
7	87.	0.0399	0.0511	0.2067	0.0074
9	50.7	0.0672	0.0864	0.3527	0.0043
Displacement-based model (DB)					
No of Elements	LIP	ε_{c20}	ε_{cc20}	ε"	bs
8	229	0.006	0.007	0.080	0.012
16	114.2	0.010	0.012	0.158	0.006
32	57.1	0.018	0.023	0.3141	0.003

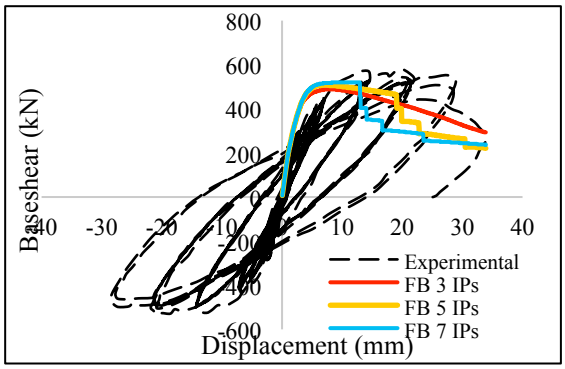

Figure 16 Monotonic response of specimen No. 3 using FB after applying material regularization only for concrete material.

Applying material regularization only for concrete failed to address the mesh-dependent response, as shown in

Figure **16** and Figure 17. The ultimate drift capacity for FB with 3, 5, and 7 IPs is different. Specimen No 3 and FL3 showed the onset of a significant concrete spalling at a drift of 1.21% (9.7 mm) and 2.79 % (102 mm), respectively; therefore, regularizing only the concrete material tackles localization issues up to those drift levels. Furthermore, applying material regularization only to steel material failed to tackle the mesh-dependent response, as shown in Figure 18 and Figure19. However, this partial regularization successfully tackled the localization or sudden drop of strength (localization of steel) observed in the non-regularized

response (Figure 13-Figure 16).

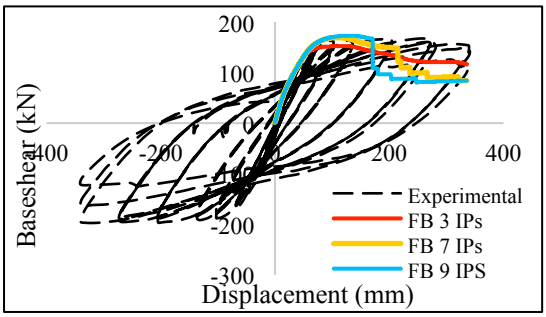

Figure 17 Monotonic response of specimen FL3 using FB after applying material regularization only for concrete material.

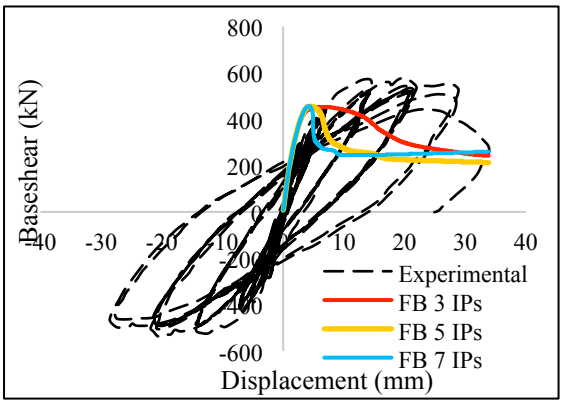

Figure 18 Monotonic response of specimen No. 3 using FB after applying material regularization only for steel material.

The most recent way is based on regularizing steel and concrete materials for fiber beam-column models. As shown in Figure 20 and Figure21, the response using FB elements is objective for all integration points. Furthermore, the ultimate strength of the specimen No 3 obtained from the experiment is 578 kN, whereas the estimated base shear using non-regularized FB with 7 IPs was 465 kN, which has a 19.31% error. When regularization was applied for both materials, the ultimate strength was 508 kN, with a 12.56% error (see Figure 20).

For the second specimen, FL3, the ultimate strength obtained from the experiment was 167.3 kN, whereas the estimated base shear using non-regularized FB with 7 IPs was 154.15 kN, which has a 7.86 % error. When both materials' regularization has been applied, the ultimate strength becomes 168.33 kN, with a 0.61 % error (see Figure21). From the above results, it is seen that the localization issue underestimates the maximum strength of the member subjected to high axial load.

As illustrated in Figure22 and Figure 23, the DB element with regularized steel and concrete material produced an objective response for all types of mesh refinement. For column No 3, the estimated base shear using non-regularized DB with 16 elements is 472.612 kN, which is an 18.3 % error, whereas the ultimate strength is 501.83 kN for the fully regularized, with a 13.2 % error (see Figure22).

For the second specimen FL3, the ultimate strength of the column obtained from the experiment is 167.3 kN, whereas the estimated based share using non-regularized DB with 16 elements is 155.8 kN, which has a 6.83 % error. For the fully regularized, the ultimate strength is 164.05 kN, which has a 1.94 % error (see Figure 23).

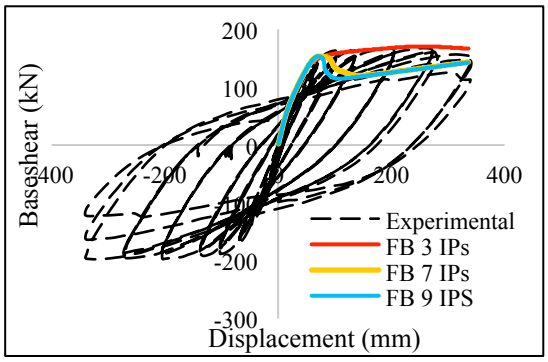

Figure19 Monotonic response of specimen FL3 using FB after applying material regularization only for steel material.

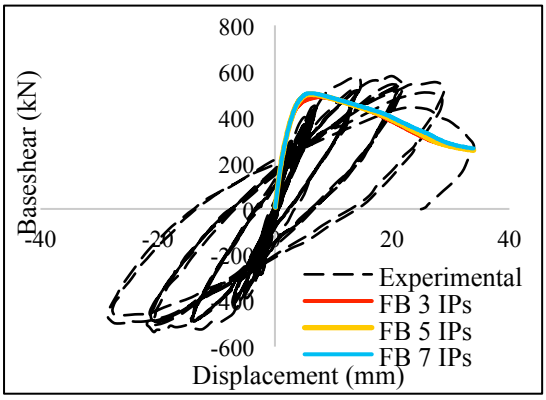

Figure 20 Monotonic response of specimen No. 3 using FB after applying material regularization for both concrete and steel materials.

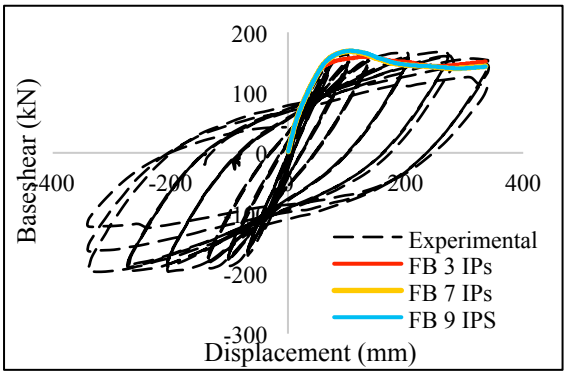

Figure21 Monotonic response of specimenFL3 using FB after applying material regularization for both concrete and steel materials.

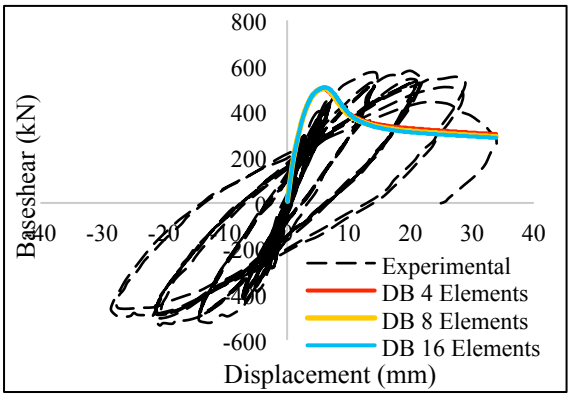

Figure22 Monotonic response of specimen No. 3 using DB after applying material regularization for both concrete and steel materials.

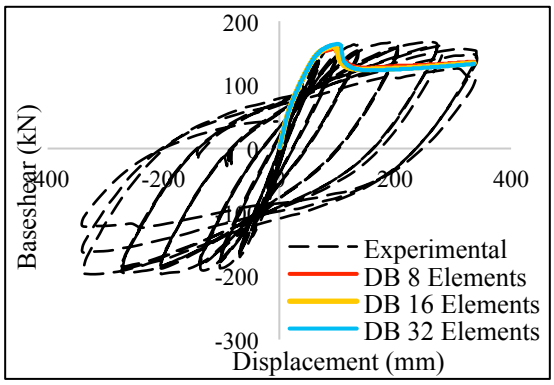

Figure 23 Monotonic response of specimen FL3 using DB after applying material regularization for both concrete and steel materials.

4. CONCLUSIONS

The research study offers the following results based on the experimentally tested cantilever columns for the section exhibiting strain-softening and strain-hardening behavior. For strain-hardening behavior, the distributed force-based fiber models with one element per member provide an accurate response. However, the distributed displacement-based fiber models require several elements per member to capture the actual inelastic response. Furthermore, in the distributed displacement-based fiber models, the rate of convergence in the local moment-curvature response is slow compared to the global force-deformation response. For sections exhibiting strain-softening behavior, both distributed force-based and displacement-based fiber models produce non-objective responses.

The study identified two types of localization in the fiber models: linear softening and sudden loss of strength resulting from concrete softening and steel localization, respectively. Furthermore, if linear softening and sudden loss of strength are observed, it is recommended to employ regularization of

steel and concrete materials to accurately capture the non-linear response.

CONFLICT OF INTEREST

The authors declare that there is no conflict of interest.

ACKNOWLEDGMENTS

The work described in this paper was prepared as a part of MSc thesis submitted in AAiT, AAU in 2019. The authors acknowledge the financial support from AAU and DBU.

REFERENCES

[1] Tauce,r F., Spacon,e E. and Filippou F., "*A fiber beam-column element for seismic response analysis of reinforced concrete structures"*, Report No. UCB/EERC-91/17, Earthquake Eng. Research Center, University of California at Berkeley, CA, December 2014, 1991.

[2] Neuenhofer, A. and Filippou, F.C., "*Evaluation of Nonlinear Frame Finite-Element Models*", Journal of Structural Engineering, vol. 123, no. 7, 1997.

[3] Coleman, E., and Spacone, J., "*Localization Issues in Force-Based Frame Elements*", Journal of Structural Engineering, vol. 127, no. 11, 2017, pp. 1257–1265.

[4] Calabrese, A., Almeida, J.P. and Pinho R., "*Numerical Issues in Distributed Inelasticity Modeling of RC Frame Elements for Seismic Analysis*", Journal of Earthquake Engineer*ing*, vol. 14, no. 51, 2010, pp. 38–68.

[5] Li, S., Zha,i C.H. and Xie, L.L., "*Evaluation of Displacement-Based, Force-Based and Plastic Hinge Elements for Structural Non-Linear Static Analysis*", Advances in Structural Engineering, vol. 15, no. 3, 2012, pp. 477–488.

[6] Pantò, B., Rapicavoli, D., Caddemi, S. and Caliò I., "*A smart Displacement Based (SDB) Beam Element with Distributed Plasticity*", Applied Mathematical Model, vol. 44, 2017, pp. 336–356.

[7] Pantò, B., Rapicavoli, D., Caddemi, S. and Caliò, I., "*A Fibre Smart Displacement Based (FSDB) Beam Element for the Nonlinear Analysis of Reinforced Concrete Members*", International Journal Non-Linear Mechanics, vol. 117, 2019.

[8] Filippou, F.C. and Fenves, G.L., "*Methods of Analysis for Earthquake-Resistant Structures", Earthquake Engineering: From Engineering Seismology to Performance-Based Engineering",* Bozorgnia Y. and Bertero V. V., eds, Chap. 6, CRC Press, 2004, pp. 316–393.

[9] Kositić, S.M. and Deretić-Stojanović, B., "*Fiber Element Formulation for Inelastic Frame Analysis*", Building Materials and Structures, vol. 59, no. 2, 2016, pp. 3–13.

[10] Jansen, D.C. and Shah, S.P., "*Effect of Length on Compressive Strain Softening of Concrete*", Journal of Engineering Mechanics, vol. 123, no. 1, 1997, pp. 25–35.

[11] Bazant, Z.P., Belytschko, T. and Chang, T.P., "*Continuum Theory for Strain-Softening*", Journal of Engineering Mechanics, vol. 110, no. 12, 1984, pp. 1666–1692.

[12] Zeris, C.A and Mahin, S.A., "*Analysis of Reinforced Concrete Beam-Columns under Uniaxial Excitation*", Journal of Structural Engineering, vol. 114, no. 4, 1988, pp. 804–820.

[13] Scott, M.H. and Fenves, G.L., "*Plastic Hinge Integration Methods for Force-Based Beam–Column Elements*", Journal of Structural Engineering, vol. 132, no. 2, 2006, pp. 244–252.

[14] Kent, D.C. and Park, R., "*Flexural Members with Confined Concrete*", Journal of the Structural Division Proc. of the American Society of Civil Engineers, vol. 97, no. 7, 1971, pp. 1969–1990.

[15] Pugh, J.S., "*Numerical Simulation of Walls and Seismic Design Recommendations for Walled Buildings*", PhD dissertation, University of Washington, 2012.

[16] Ashtari, S., "*Evaluating the Performance-Based Seismic Design of RC Bridges According to the 2014 Canadian Highway Bridge Design Code*", PhD Dissertation, University of British Columbia, 2018.

[17] Menegotto, M. and Pinto, P.E., "*Method of Analysis for Cyclically Loaded RC Plane Frames Including Changes in Geometry and Non-Elastic Behavior of Elements under Combined Normal Force and Bending*", Proceedings of IABSE Symposium on Resistance and Ultimate Deformability of Structures Acted on by Well Defined Repeated Loads, 1973.

[18] McKenna, F., Fenves, G.L. and Scott M.H., "*Open System for Earthquake Engineering Simulation*", University of California, Berkeley, 2000. http://opensees.berkeley.edu/

[19] Mander, J.B., Priestley, M.J.N. and Park R., "*Theoretical Stress-Strain Model for Confined Concrete*," Journal of Structural Engineering, vol. 114, no. 8, 1988, pp. 1804–1826.

[20] Priestley, M.J.N., Seible, F. and Calvi, G.M., "*Seismic Design and Retrofit of Bridges",* John Wiley & Sons, 1996.

[21] Fllippou, E., Popov, P. and Bertero, V.V, "*Effects of Bond Deterioration on Hysteretic Behavior of Reinforced Concrete Joints*", Earthquake Engineering Research Center, Report No. UCB/EERC-83/19, 1983.

[22] Kunnath, S.K., El-Bahy, A., Taylor, A. and Stone, W., "*Cumulative Seismic Damage of Reinforced Concrete Bridge piers*", Technical Report NCEER-97-0006, National Center for Earthquake Engineering Research, 1997.

[23] Wong, Y., Paulay, T. and Priestley, M., "*Response of Circular Reinforced Concrete Columns to Multi- Directional Seismic Attack*", ACI Struct J, vol. 90, no. 2, 1993, pp. 180–191.

[24] Kowalsky, M.J., Priestley M.J.N. and Seible, F., "*Shear and Flexural Behavior of Lightweight Concrete Bridge Columns in Seismic Regions*", ACI Structural Journal, vol. 96, no. 1, 1999, pp. 136–148.